Geophysical Journal International

Geophys. J. Int. (2020) **222,** 1034–1045
Advance Access publication 2020 April 30
GJI Geomagnetism, rock magnetism and palaeomagnetism

doi: 10.1093/gji/ggaa173

Magnetic anisotropy reveals Acadian transpressional fabrics in an Appalachian ophiolite (Thetford Mines, Canada)

Anita Di Chiara,[1,*] Antony Morris,[1] Mark W. Anderson,[1] Luca Menegon[1,†] and Alain Tremblay[2]

[1]*School of Geography, Earth and Environmental Sciences, University of Plymouth, Drake Circus, Plymouth PL48AA, UK. E-mail: amorris@plymouth.ac.uk*
[2]*Département des Sciences de la Terre et de l'Atmosphère, Université du Québec à Montréal, H2X 3Y7 Canada*

Accepted 2020 April 7. Received 2020 April 2; in original form 2019 November 19

SUMMARY

Magnetic anisotropy has proved effective in characterizing primary, spreading-related magmatic fabrics in Mesozoic (Tethyan) ophiolites, for example in documenting lower oceanic crustal flow. The potential for preservation of primary magnetic fabrics has not been tested, however, in older Palaeozoic ophiolites, where anisotropy may record regional strain during polyphase deformation. Here, we present anisotropy of magnetic susceptibility results from the Ordovician Thetford Mines ophiolite (Canada) that experienced two major phases of post-accretion deformation, during the Taconian and Acadian orogenic events. Magnetic fabrics consistent with modal layering in gabbros are observed at one locality, suggesting that primary fabrics may survive deformation locally in low strain zones. However, at remaining sites rocks with different magmatic origins have consistent magnetic fabrics, reflecting structurally controlled shape preferred orientations of iron-rich phases. Subhorizontal NW-SE-oriented minimum principal susceptibility axes correlate with poles to cleavage observed in overlying post-obduction, pre-Acadian sedimentary formations, indicating that the magnetic foliation in the ophiolite formed during regional NW-SE Acadian shortening. Maximum principal susceptibility axes plunging steeply to the NE are orthogonal to the orientation of regional Acadian fold axes, and are consistent with subvertical tectonic stretching. This magnetic lineation is parallel to the shape preferred orientation of secondary amphibole crystals and is interpreted to reflect grain growth during Acadian dextral transpression. This structural style has been widely reported along the Appalachian orogen, but the magnetic fabric data presented here provide the first evidence for transpression recorded in an Appalachian ophiolite.

Key words: Magnetic properties; North America; Magnetic fabrics and anisotropy; Folds and folding.

1 INTRODUCTION

Ophiolites are fragments of oceanic lithosphere emplaced onto continental margins during orogenesis and frequently preserve evidence of their intraoceanic tectonomagmatic evolution by seafloor spreading. Palaeomagnetic analyses have been used extensively to decipher the tectonic rotation history of various ophiolites, principally in the Tethyan realm (e.g. MacLeod *et al.* 1990; Morris *et al.* 1998; Inwood *et al.* 2009; Maffione *et al.* 2015), and magnetic fabric (anisotropy) techniques have previously been used to understand the development of accretion-related petrofabrics in ophiolitic rocks. For example, in the slow spreading rate, Late Cretaceous Troodos ophiolite of Cyprus, anisotropy of magnetic susceptibility (AMS) has been used to determine both the emplacement directions of sheeted dykes (Staudigel *et al.* 1992) and the pattern of magmatic flow in lower crustal gabbros (Abelson *et al.* 2001), along with their relationship to the well-documented spreading structure of the ophiolite (MacLeod *et al.* 1990; Allerton & Vine 1991; Morris & Maffione 2016). Similarly, AMS has been used in the fast-spreading rate, Late Cretaceous Oman ophiolite to examine dyke emplacement (Rochette *et al.* 1991) and magmatic fabric development in layered and foliated gabbros (Yaouancq & MacLeod 2000; Meyer 2015). In the case of lower crustal gabbros in Oman, alteration (involving serpentinization of olivine crystals) has resulted in the production of secondary magnetite grains, but their orientation and distribution have been controlled by the crystallographic orientation of primary

* Now at: Geosciences Research Division, Scripps Institution of Oceanography, University of California, San Diego, La Jolla, CA 92093-0220, USA.
† Now at: Department of Geosciences, University of Oslo, P.O. Box 1048, Blindern, 0316 Oslo, Norway.

© The Author(s) 2020. Published by Oxford University Press on behalf of The Royal Astronomical Society.

Downloaded from https://academic.oup.com/gji/article-abstract/222/2/1034/5827533 by guest on 02 July 2020

silicate phases, leading to AMS fabrics that still act as a reliable proxy for primary magmatic fabrics (Yaouancq & MacLeod 2000; Meyer 2015).

Here, we present magnetic fabric results from the more ancient, Thetford Mines ophiolite in the Canadian Appalachians. This Ordovician ophiolite formed in a forearc setting at 480 Ma (Laurent & Hébert 1989; Olive *et al.* 1997; Whitehead *et al.* 2000) and was obducted onto the Laurentian margin shortly afterwards (470–460 Ma; Tremblay *et al.* 2009). It experienced two Palaeozoic deformation episodes during regional contraction and shortening (Tremblay *et al.* 2009). We demonstrate that in this case magnetic fabrics within most of the ophiolite reflect the latest Acadian phase of regional deformation (related to accretion of Avalonia onto the Laurentian margin), rather than seafloor-spreading processes, with primary magmatic fabrics being obliterated by a pervasive tectonic overprint during folding in a dextral transpressive regime.

2 THE THETFORD MINES OPHIOLITE

The Thetford Mines ophiolite is located in the southern Québec Appalachians belt that consists of three lithotectonic assemblages: (1) the Cambrian-Ordovician Humber zone, a remnant of the Laurentian passive continental margin; (2) the Cambrian-Ordovician Dunnage zone (Williams 1979), a remnant of the Iapetus Ocean and (3) the Silurian-Devonian Gaspé Belt (Tremblay & Pinet 2005), representing a sedimentary cover sequence. The Humber and Dunnage zones were amalgamated during the Ordovician Taconian orogeny, involving closure of the Iapetus Ocean and emplacement of a large ophiolite nappe (now preserved in the dismembered Southern Québec ophiolites, Tremblay & Castonguay 2002; Tremblay & Pinet 2005). The Gaspé Belt successor basin and underlying Dunnage zone were subsequently regionally deformed and metamorphosed during the Devonian Acadian orogeny (Tremblay & Pinet 2005).

Oceanic rocks of the Dunnage zone in the area of the present study consist of the following assemblages (Fig. 1): (1) the Thetford Mines ophiolite; (2) the Saint-Daniel Mélange and (3) sedimentary rocks of the Magog Group. The ophiolite has a boninitic geochemistry and is inferred to have formed in a forearc setting (Laurent & Hébert 1989; Olive *et al.* 1997; Tremblay *et al.* 2009). U/Pb dating of plagiogranites in the ophiolite indicate formation at 479 ± 3 Ma (Whitehead *et al.* 2000), whereas amphibole and mica ages from its metamorphic sole yielded ages of 477 ± 5 and 469–461 Ma, respectively (Whitehead *et al.* 1995; Castonguay *et al.* 2001). This indicates that oceanic detachment of the ophiolite occurred immediately after crustal formation. Debris flow deposits of the Saint-Daniel Mélange and the overlying Magog Group rocks are both interpreted to represent a sequence of forearc basin sediments developed on the ophiolitic basement (Schroetter *et al.* 2006), with a major erosional unconformity at the base.

The Thetford Mines ophiolite is approximately 40 km long and 10–15 km wide, and may be divided into the Thetford Mines and AHM (Fig. 1), with the former dominated by a ∼5 km thick mantle section and the latter by a thicker crustal sequence of plutonic and extrusive rocks. Plutonic sequences in both massifs consist of dunitic, pyroxenitic and gabbroic cumulates, cross-cut by mafic and ultramafic dykes, which grade up locally into a poorly exposed sheeted dyke complex (Tremblay *et al.* 2009). The extrusive sequences are dominated by boninitic lava flows and pillow lavas and felsic pyroclastic rocks.

Structural reconstructions suggest that the seafloor spreading history of the Thetford Mines ophiolite involved development of an oceanic core complex, marked by detachment faults that exhumed the upper mantle and lower crustal sections to the seafloor (Tremblay *et al.* 2009), as seen in slow-spreading systems in the present-day Atlantic and Indian Oceans (e.g. Blackman *et al.* 2011; MacLeod *et al.* 2017). Structures associated with this early phase of spreading-related intraoceanic deformation were then superimposed by syn-obduction NW-verging shear zones and folds associated with the Taconian orogeny and then by post-obduction NW-verging folds and faults developed during the Acadian orogeny (Figs 1b and c). This last regional deformation event resulted from collision between the Avalonia terrane and the irregular margin of Laurentia and its Taconian accreted terranes in the Devonian (Malo & Kirkwood 1995; Sacks *et al.* 2004)

3 SAMPLING AND METHODS

Samples were collected from 12 sites representing four localities in the Thetford Mines ophiolite (Fig. 1) using a portable rock drill. The orientation of drill cores was measured using both magnetic and sun compasses, along with the orientation of any magmatic structures present. Layered gabbros were sampled at three sites in the southwest sector of the ophiolite (sites TM05–07; Fig. 1), along a road cut adjacent to the shore of Lac Breeches, where a clear and consistent magmatic foliation defined by variations in modal composition was observed between sites. Nine sites were collected in the northeast of the study area near the Mount Adstock-Ham Massif (AHM; Fig. 1), north of Lac St. François. Site TM10 was sampled in pillow lavas and tabular lava flows sampled as sites TM11 and 12, with pillows and flows having very similar orientations. Sites TM02–04 were collected in a road cut where subvertical dykes (sites TM03 and 04) cut through well-developed, elongate pillow lavas (site TM02) at a high angle. Site TM09 sampled elongate pillow lavas exposed in a disused quarry, and site TM08 was located in serpentinized dunite adjacent to Lac Rond. The average orientations of pillow lavas and dykes were determined from multiple measurements at each site for use as structural corrections, and the way-up of lavas noted (based on typical pillow morphologies). All sampled lavas had subvertical or overturned orientations, dipping ∼80°–105° and appear tectonically stretched (Table 1). Finally, a roadside exposure of massive gabbro was sampled at site TM01. No primary structures were observed at either this site or in the serpentinized dunite (site TM08).

We measured the anisotropy of low-field magnetic susceptibility (AMS) of 145 standard (11 cm^3) samples using an AGICO KLY-3S Kappabridge. AMS is a petrofabric tool that reflects the preferred orientation of grains, grain distributions and/or the crystal lattices of minerals that contribute to the magnetic susceptibility of a rock (e.g. Tarling & Hrouda 1993; Borradaile & Jackson 2004). AMS corresponds to a second-order tensor that may be represented by an ellipsoid specified by the orientation and magnitude of its principal axes (k_{max}, k_{int} and k_{min}, being the maximum, intermediate, and minimum susceptibility axes respectively, Tarling & Hrouda 1993). The AMS of a rock may result from contributions from diamagnetic, paramagnetic and ferromagnetic minerals. Susceptibility tensors and associated eigenvectors and eigenvalues were calculated using AGICO Anisoft 4.2 software. The relative magnitude of the susceptibility axes defines the shape of the AMS ellipsoid, which can be: (1) isotropic ($k_{min} = k_{int} = k_{max}$) when crystals are not aligned preferentially and when strongly magnetic grains have

Downloaded from https://academic.oup.com/gji/article-abstract/222/2/1034/5827533 by guest on 02 July 2020

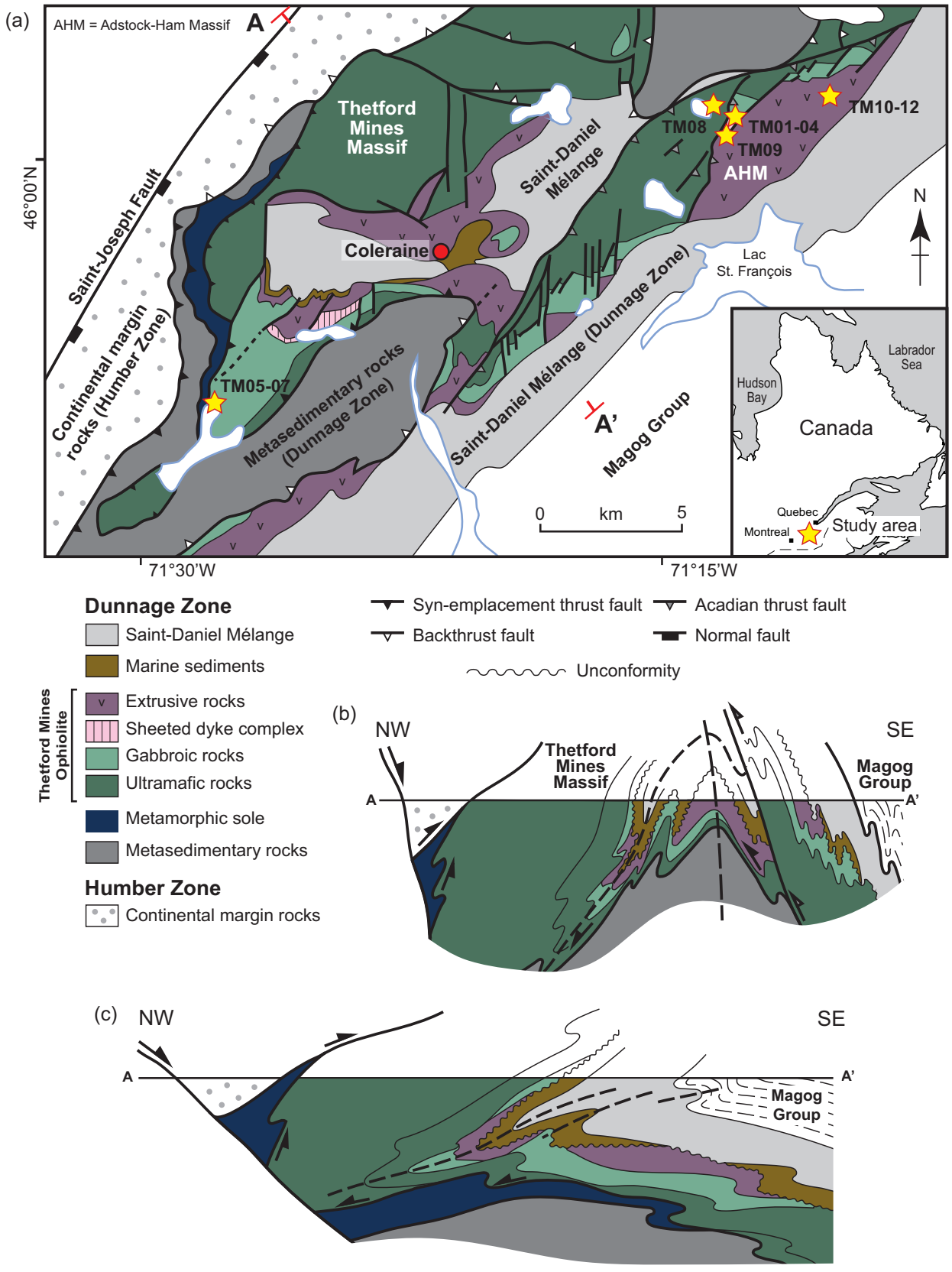

Figure 1. (a) Simplified geological map of the Thetford Mines ophiolite showing site locations (after Pagé *et al.* 2009); (b) structural profile along line A–A′ on the geological map (after Tremblay *et al.* 2009) showing the current geometry of the ophiolite resulting from two superimposed folding events, with upright folds due to the final, Acadian phase of regional deformation and (c) schematic cross-section along the same line illustrating retro-deformation of the ophiolite and restoration to its inferred geometry prior to Acadian folding (after Tremblay *et al.* 2009).

Downloaded from https://academic.oup.com/gji/article-abstract/222/2/1034/5827533 by guest on 02 July 2020

Table 1. AMS results from the Thetford Mines ophiolite.

Site	Location	Northing	Easting	Description	Unit orientation	N	Mean k (x 10^{-6} SI)	Normalized principal susceptibilities			Principal axes				
								k_{max}	k_{int}	k_{min}	k_{max}	k_{int}	k_{min}	P_J	T
TM01	Lac St Francois	5 097 790	326 698	Massive gabbro	–	10	430	1.029	1.005	0.966	044/55	265/28	164/20	1.099	0.220
TM02	Lac St Francois	5 097 747	327 185	Pillow lava	210/105 (O/T)	16	480	1.007	1.000	0.993	057/66	239/24	149/01	1.015	0.105
TM03	Lac St Francois	5 097 728	327 210	Dyke cutting TM02	166/85	13	492	1.008	1.000	0.992	083/67	236/21	330/10	1.016	−0.003
TM04	Lac St Francois	5 097 732	327 205	Dyke cutting TM02	166/88	14	505	1.007	1.001	0.992	088/78	242/11	333/05	1.016	0.178
TM08	Lac Rond	5 098 226	325 902	Serpentinized dunite	–	5	71 100	1.126	1.019	0.855	021/67	248/16	154/16	1.339	0.225
TM09	Lac St Francois	5 097 330	326 845	Pillow lavas	278/98 (O/T)	15	1050	1.035	1.001	0.964	052/81	266/08	176/05	1.093	0.290
TM10	Mount Adstock	5 098 523	329 636	Pillow lavas	115/85	10	438	1.011	1.005	0.984	106/73	214/05	305/16	1.030	0.549
TM11	Mount Adstock	5 098 523	329 636	Lava flow	115/85	10	392	1.010	1.003	0.987	097/66	213/11	307/21	1.025	0.359
TM12	Mount Adstock	5 098 523	329 636	Lava flow	115/85	9	532	1.030	1.004	0.967	071/69	208/16	302/14	1.068	0.224
TM05	Lac de Breeches	5 088 336	308 603	Layered gabbro	202/32	13	8840	1.014	0.999	0.987	296/10	199/33	040/55	1.040	0.147
TM06	Lac de Breeches	5 088 295	308 686	Layered gabbro	202/32	11	30 800	1.050	1.011	0.939	106/02	197/26	013/64	1.139	0.317
TM07	Lac de Breeches	5 088 280	308 801	Layered gabbro	202/32	19	503	1.011	1.003	0.986	095/04	188/43	001/47	1.029	0.299

Notes: Coordinates are UTM WGS84 datum, zone 19T; Unit orientation = dip direction/dip (O/T = overturned); N = number of specimens; k = low-field magnetic susceptibility; principal anisotropy axes given as site mean azimuth/plunge; P_J = corrected anisotropy degree and T = shape factor (Jelínek 1978).

a random distribution; (2) oblate ($k_{min} << k_{int} \approx k_{max}$) when crystal alignment defines a foliation plane; (3) triaxial ($k_{min} < k_{int} < k_{max}$); or (4) prolate ($k_{min} \approx k_{int} << k_{max}$) when crystal alignment defines a lineation. However, the presence of some minerals (e.g. single domain magnetite; Potter & Stephenson 1988) and/or interference between signals carried by different minerals may complicate the structural interpretation of AMS data. Here. we describe the strength of anisotropy using the corrected anisotropy degree (P_J; Jelínek 1978), where $P_J = 1.0$ indicates an isotropic fabric and, for exmple $P_J = 1.05$ indicates 5 per cent anisotropy. The shape of the ellipsoid is described by the shape parameter (T), where $-1.0 < T < 1.0$ with positive/negative values of T indicate oblate/prolate fabrics respectively (Jelínek 1978). We also determined the anisotropy of isothermal remanent magnetization (AIRM) for selected specimens in order to check for presence of inverse magnetic fabrics, following the methodology of Potter & Stephenson (1988). A direct field of 80 mT was applied sequentially along specimen x, y and z-axes, with alternative field (AF) demagnetization of specimens at 100 mT between IRM acquisition steps. Although higher direct fields would be required to achieve a saturation IRM, 80 mT was selected to ensure complete AF demagnetization could be achieved between field applications. Eigenvalues and eigenvectors of the AIRM tensors were calculated using the 'EigenCalc' v. 1.1.0 program of Rick Allmendinger.

Rock magnetic experiments were performed to investigate the nature of the ferromagnetic minerals contributing to the AMS. Curie temperatures were determined from the high-temperature (20–700 °C) variation of magnetic susceptibility of representative samples, measured using an AGICO KLY-3S Kappabridge coupled with an AGICO CS-3 high-temperature furnace apparatus. Curie temperatures were determined from these data using the method of Petrovský & Kapička (2006).

Isothermal remanent magnetization (IRM) acquisition experiments were conducted on representative samples using a Molspin pulse magnetizer to apply peak fields up to 800 mT with resulting IRMs measured using an AGICO JR6A fluxgate spinner magnetometer. Finally, scanning electron microscope (SEM) observations of oriented thin sections were used to further establish the source of the AMS signal. Polished thin sections were carbon coated and analysed with a JEOL 7001 FEG-SEM at the Electron Microscopy Centre of the University of Plymouth. Backscattered electron (BSE) images were acquired with 15 kV accelerating voltage and 10 mm working distance. Energy dispersive spectroscopy (EDS) point analysis was used for phase identification. The preferred orientations of crystal long axes in BSE images were then determined using ImageJ software (Schneider *et al.* 2012) and analysed using OSXStereonet (Cardozo & Allmendinger 2013).

4 RESULTS

4.1 Rock magnetic properties

Lavas, dykes and massive gabbros of the Thetford Mines ophiolite have consistently weak low-field magnetic susceptibilities of ∼400–500 × 10^{-6} SI (Table 1 and Fig. 2). These values suggest a dominant contribution from paramagnetic silicate minerals or a combined paramagnetic and ferromagnetic signal but with <0.03 wt per cent of magnetite present (Fig. 2). In contrast, serpentinized dunite samples have much higher susceptibilities (∼70 × 10^{-3} SI) consistent with a dominantly ferromagnetic source. The temperature dependence of susceptibility in lavas and dykes

Downloaded from https://academic.oup.com/gji/article-abstract/222/2/1034/5827533 by guest on 02 July 2020

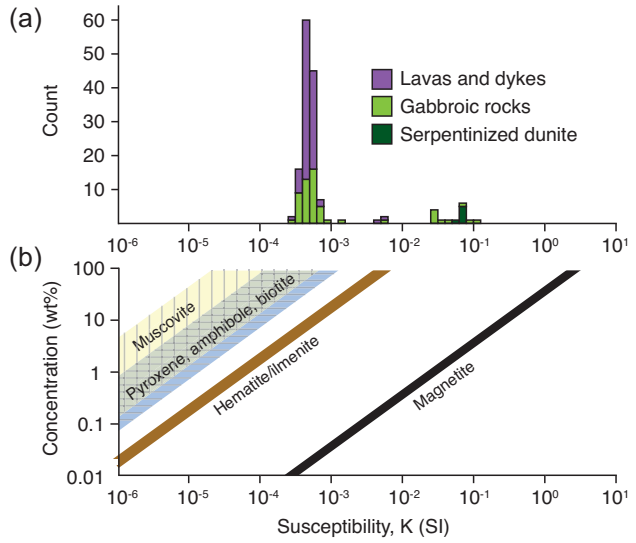

Figure 2. (a) Histogram of low-field magnetic susceptibilities for rocks of the Thetford Mines ophiolite; and (b) relationship between bulk susceptibility and mineral concentrations (wt per cent, Tarling & Hrouda 1993). Note that low susceptibilities in most of the Thetford Mines ophiolite indicate less than 0.1 wt per cent magnetite in these rocks or a major contribution from paramagnetic silicate minerals.

(Fig. 3a) shows initial decreases with temperature, consistent with a dominantly paramagnetic signal following the Curie–Weiss law (Tarling & Hrouda 1993) in these rocks, combined with a minor ferromagnetic signal with Curie temperatures of ∼570–600 °C, indicating presence of minor magnetite. Some samples show evidence for magnetite production during laboratory heating, shown by higher susceptibilities during the cooling cycle and by peaks in susceptibility above 400 °C (Fig. 3a). IRM experiments on these rocks (Fig. 3b) confirm the presence of a low coercivity phase (most likely to be magnetite), but with saturation IRMs that are very low in intensity (<100 mA m^{-1}) and again consistent with low weight percentages of magnetite. In contrast, thermomagnetic curves for samples of layered gabbro (sites TM05–07) show evidence for susceptibilities dominated by a ferromagnetic signal with magnetite Curie temperatures of ∼580 °C and with no discernable contribution from paramagnetic phases (Fig. 3a), although saturation IRM values are again lower than comparable rocks in younger (Tethyan) ophiolites or in drill core samples from the lower oceanic crust (e.g. Morris *et al.* 2016; MacLeod *et al.* 2017).

Serpentinized dunites sampled at site TM08 have Curie temperatures of ∼580 °C and IRM curves showing presence of a low coercivity phase (Fig. 3), indicating production of near stoichiometric magnetite in these rocks during serpentinization. The degree of serpentinization, S, may be determined using a linear, inverse correlation between S and bulk density (ρ) defined by Miller & Christensen (1997):

$$S = (3.3 - \rho)/0.785 \times 100 \text{ per cent}$$

Densities of samples from site TM08 range from 2.62 to 2.71 g cm^{-3}, corresponding to serpentinization degrees of 69–86 per cent. Bulk susceptibilities of 0.059–0.079 SI correspond to volume fractions of magnetite of ∼2.0–2.5 per cent (Thompson & Oldfield 1986). These values are consistent with relationships derived from an extensive data base of abyssal and ophiolitic serpentinized peridotites reported by Maffione *et al.* (2014).

4.2 Magnetic anisotropy results

The majority of individual specimens exhibit oblate AMS fabrics, with a mean T value of 0.33, although 22 per cent of specimens have prolate fabrics with a mean T value of −0.18 (Fig. 4a and Table S1, Supporting Information). The strength of anisotropy is described by the corrected anisotropy degree, P_J, and ranges from 1.01 to 1.60 for individual specimens (Fig. 4a). Mean P_J values vary by lithology, from 1.04 in the lavas and dykes, through 1.07 for gabbros, to 1.34 in the serpentinized dunites (where high values may reflect a strong distribution anisotropy carried by magnetite within serpentinized olivine crystals). There is no preferred relationship between P_J and T (Fig. 4a), and no correlation between P_J and mean susceptibility (Fig. 4b), indicating that the degree of anisotropy is not dependent on variations in ferromagnetic concentration.

At a site level, clustering of k_{max} and k_{min} axes define the magnetic lineation and the pole to the magnetic foliation, respectively. Oblate fabrics are characterized by clustered k_{min} axes orthogonal to girdle distributions of k_{max} and k_{int} axes, whereas prolate fabrics by clustered k_{max} axes orthogonal to girdle distributions of k_{int} and k_{min} axes. In triaxial fabrics, the three principal susceptibility axes form distinct groups.

In the layered gabbro sites, k_{min} axes coincide with the pole to the magmatic layering observed in the field, with a girdle distribution of k_{max} and k_{int} axes, defining an oblate fabric parallel to the modal layering (Fig. 5a). Combined with evidence for magnetite dominating the rock magnetic properties of these rocks, this suggests that the fabric is due to the shape-preferred orientation of magnetite grains distributed in the plane of layering. This fabric compares well with those observed in layered gabbros in other ophiolites [e.g. in Oman (Meyer 2015); Fig. 5c], and indicates that magmatic fabrics are preserved at this locality.

At the majority of other sites fabrics are triaxial and marked by discrete clusters of principal axes, with the exception of the massive gabbros sampled at site TM01 where a prolate site-level fabric is developed (Fig. 6). At all these sites, k_{min} axes are subhorizontal/shallowly plunging and aligned NW-SE whereas k_{max} axes plunge steeply to the NE. This arrangement of principal axes is consistent across all sites regardless of both their magmatic origin and the orientation of associated magmatic structures (where observable in the field), with pillow lavas, lava flows, dolerite dykes, massive gabbros and serpentinized dunites all sharing the same fabric style. This strongly suggests that the fabric in these rocks developed tectonically and does not reflect primary magmatic processes. The origin of this tectonic fabric is discussed below by comparison with the regional structural framework of the Thetford Mines ophiolite and the Canadian Appalachians in general.

AIRM ellipsoids (Table S2, Supporting Information) show widely varying degrees of alignment with the orientation of the corresponding AMS principal susceptibility axes. Fig. 7(a) shows AIRM principal axes rotated to align the corresponding k_{max} axes to the vertical and k_{min} axes to a horizontal north direction to allow comparison of the degree of alignment of AIRM and AMS fabrics, and Fig. 7(b) shows the relationship between the angular difference between maximum anisotropy axes and the intensity of IRM acquired at 80 mT. Specimens from the layered gabbros have angular differences of <25°, confirming presence of normal AMS fabrics in these rocks. Serpentinized dunite from site TM08 shows near perfect alignment of AMS and AIRM fabrics in these magnetite-rich rocks, again confirming presence of a normal AMS fabric. Specimens from all other sites, however, show widely scattered AIRM axes, showing no correspondence between weakly developed AIRM

Downloaded from https://academic.oup.com/gji/article-abstract/222/2/1034/5827533 by guest on 02 July 2020

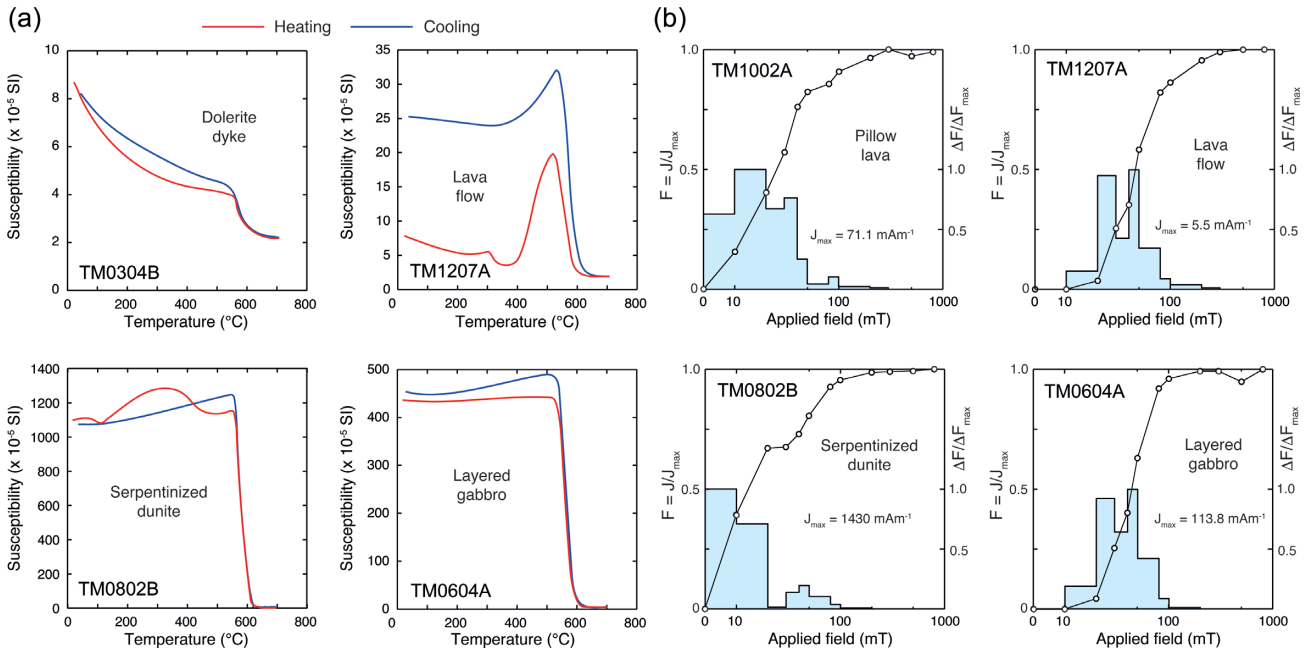

Figure 3. Representative examples of (a) the variation of low-field magnetic susceptibility with temperature and (b) isothermal remanent magnetization acquisition curves for rocks from the Thetford Mines ophiolite.

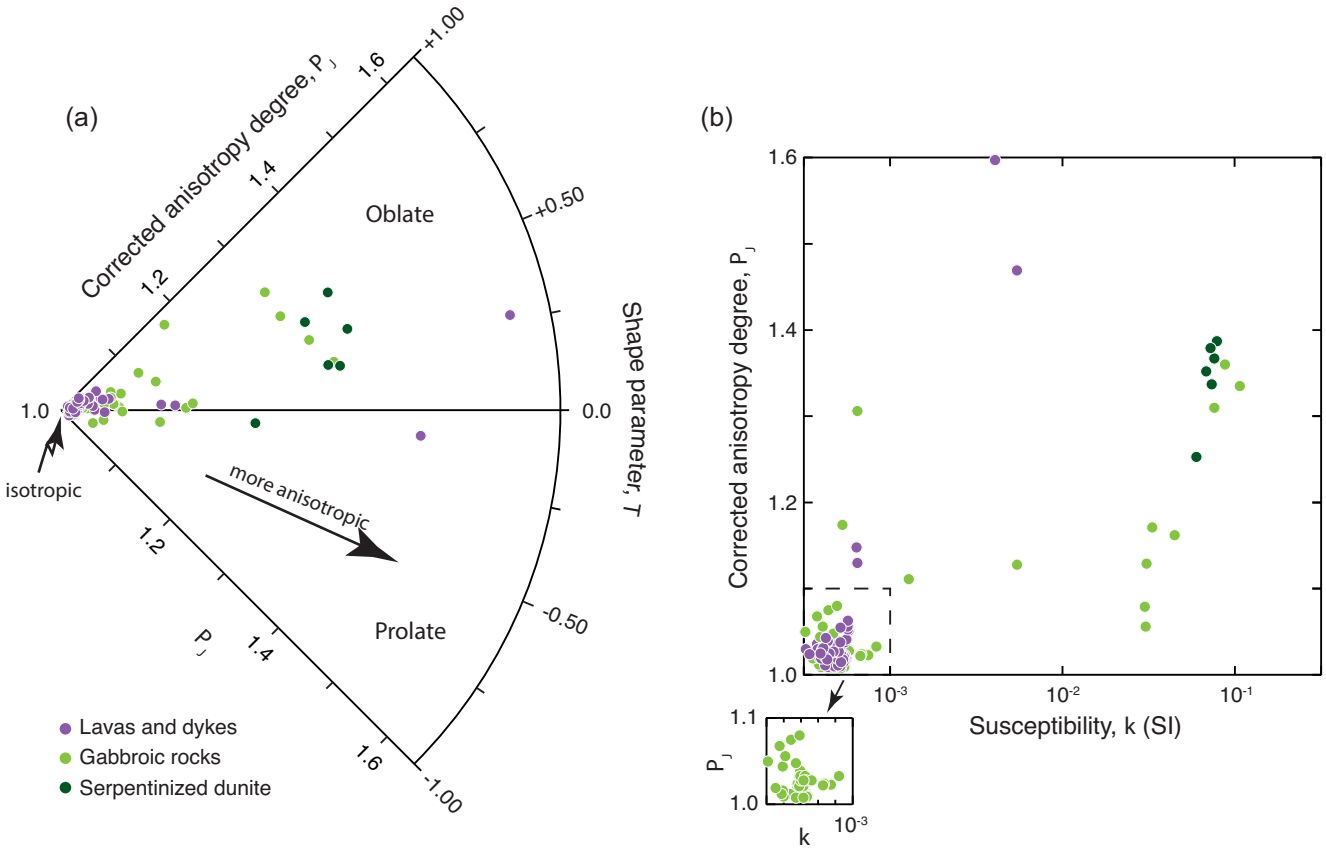

Figure 4. (a) Borradaile–Jackson polar plot of corrected anisotropy degree, P_J, and shape parameter, T (Jelínek 1978; Borradaile & Jackson 2004) and (b) plot of corrected anisotropy degree, P_J, against bulk susceptibility.

Downloaded from https://academic.oup.com/gji/article-abstract/222/2/1034/5827533 by guest on 02 July 2020

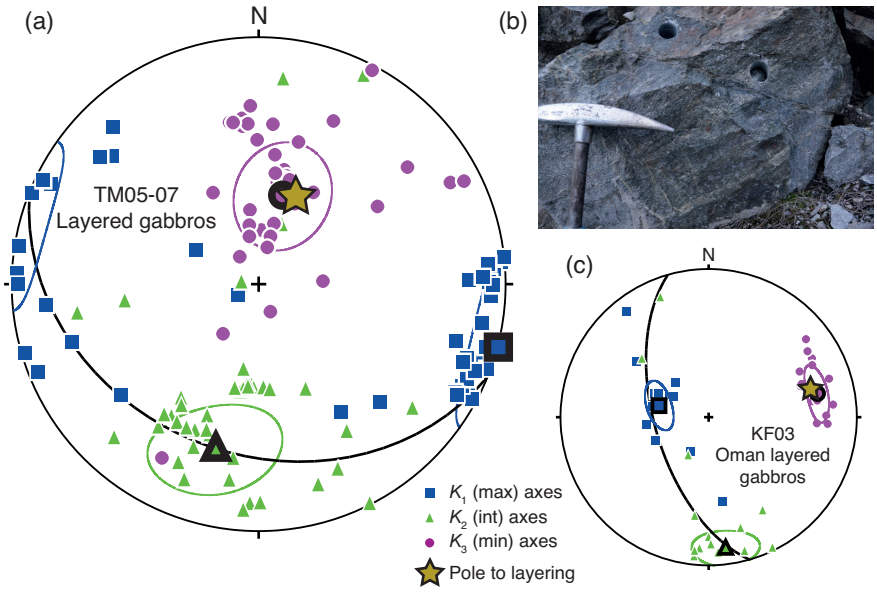

Figure 5. (a) Equal area stereographic projection of principal anisotropy axes of samples from layered gabbros in the Thetford Mines ophiolite. Principal directions of the mean tensor are represented by large symbols, with ellipses representing 95 per cent confidence regions calculated according to Jelínek (1978). Great circle/star = plane/pole to plane of modal compositional layering measured in the field and shown in (b) and (c) equal area stereographic projection of an example of AMS data from layered gabbros in the Oman ophiolite (Meyer 2015). Symbols as in (a).

fabrics carried by magnetite and AMS fabrics dominated by silicate phases (see below).

5 DISCUSSION

5.1 Source of the AMS signal

The dominantly triaxial AMS fabrics in the Thetford Mines ophiolite samples are likely to reflect a combination of flattening during deformation (producing clustering of k_{min} axes) and a preferred orientation of the long axes of minerals (producing clustering of k_{max} axes). The source of the dominant fabric signal in these generally fine-grained rocks may be determined via examination of oriented thin sections using backscatter SEM microscopy. These observations reveal that k_{max} axes in the lavas are parallel to the preferred orientation of the long axes of secondary amphibole crystals (Fig. 8), inferred to represent an alignment of crystal *c*-axes. This supports a secondary origin for the observed fabrics involving grain growth during deformation, resulting in alignment of newly formed amphibole crystals parallel to the long axis of the finite-strain ellipsoid. Biedermann *et al.* (2015) recently showed that k_{max} axes in single amphibole crystals lie parallel to their crystallographic *b*-axes, rather than their *c*-axes. However, Biedermann *et al.* (2018) demonstrated that in rocks where amphibole c-axes are preferentially aligned (their 'c-fiber texture') then mean AMS k_{max} axes lie parallel to the lineation defined by the preferred alignment of crystals.

Fabrics due to the growth of secondary amphiboles during alteration and deformation may also account for the low quantities of magnetite present in the Thetford Mines ophiolite compared to other ophiolites and oceanic crustal rocks, as magnetite may be destroyed during alteration, mobilizing iron that then becomes incorporated into the newly formed amphibole crystals.

5.2 Implications of the magnetic fabric results for the regional tectonic regime

The consistent AMS fabric between sites that have different magmatic origins in the NE of the study area is consistent with complete tectonic overprinting of any primary fabrics in this part of the ophiolite. In contrast, the layered gabbro locality preserves magnetic fabrics that parallel the modal layering observed in the field (Fig. 5a). This clearly shows that primary fabrics of magmatic origin are preserved in the SW part of the Thetford Mines ophiolite, presumably within a low-strain domain. Alternatively, the moderate dip of the layered gabbros may indicate a position close to a hinge zone within the major upright fold structures that dominate the present-day structure (Fig. 1b), allowing this locality to escape pervasive overprinting by a tectonic fabric that developed elsewhere. The consistency of fabrics at all other sites is illustrated in Fig. 9a, which shows Kamb contoured distributions (Cardozo & Allmendinger 2013) of the k_{min} and k_{max} axes combined from all sites (excluding the layered gabbros). The origin and timing of acquisition of this tectonic fabric can be established by comparing the AMS results with fold geometries and field structural data from the wider region.

The major deformation phases in the Canadian Appalachians that could potentially produce the observed fabric are the Taconian (Ordovician) and Acadian (Devonian) orogenic events. The Taconian event resulted from closure of the Iapetus Ocean and obduction of the Southern Québec ophiolites (Pinet & Tremblay 1995; Tremblay & Castonguay 2002; Sacks *et al.* 2004). The Acadian event involved collision between the Avalonia terrane and the margin of Laurentia and its Taconian-accreted terranes, including the Thetford Mines ophiolite (Malo & Kirkwood 1995; Sacks *et al.* 2004). Acadian deformation dominates the present-day structure of the area and resulted in development of upright folds during NW-SE contraction (Fig. 1b), and is superimposed on a series of earlier SE-verging recumbent folds (Fig. 1c; Tremblay *et al.* 2009).

Downloaded from https://academic.oup.com/gji/article-abstract/222/2/1034/5827533 by guest on 02 July 2020

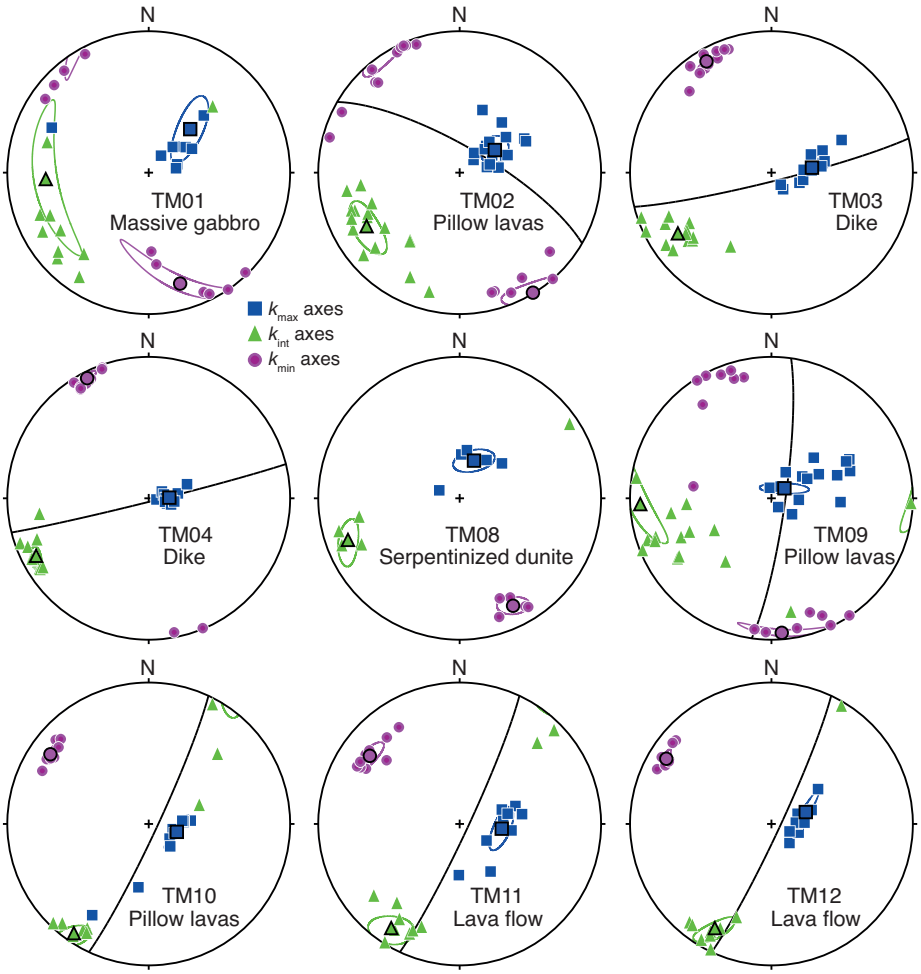

Figure 6. Site-level AMS results from the Thetford Mines ophiolite. Principal directions of mean tensors at each site are represented by large symbols, with ellipses representing 95 per cent confidence regions calculated according to Jelínek (1978). Great circles = orientation of magmatic structures measured in the field (lava and dyke planes).

The structural style of the Acadian folding is best described using field structural data from the overlying, post-obduction but pre-Acadian sedimentary sequences. Field data from St-Julien (1987) shows that poles to bedding define a great circle distribution forming a π-girdle that indicates Acadian fold axes plunging shallowly to the SW (Fig. 9b). Poles to Acadian cleavage planes are oriented NW-SE with shallow plunges, while bedding cleavage intersection lineations and fold axes observed in the field have shallow plunges to the SW (consistent with the π-axis determined from bedding data; Fig. 9c). The correlation between k_{min} axes (Fig. 9a) and poles to cleavage (Fig. 9c) strongly suggests that the tectonic fabric represented by the magnetic fabric data formed during upright folding associated with Acadian contraction.

Magnetic fabrics in folded rocks commonly show an alignment of k_{max} axes along the intersection of axial planar cleavage and primary foliation planes (e.g. bedding; Borradaile & Tarling 1981; Hrouda *et al.* 2000; Parés 2015; Fig. 10a). This relationship results from overprinting of an initial magnetic fabric (characterized by alignment of k_{min} axes perpendicular to the primary foliation) by a tectonic fabric (characterized by k_{min} axes aligned perpendicular to cleavage) (e.g. Housen *et al.* 1993). Such composite magnetic fabrics are usually dominantly oblate in shape with k_{max} axes typically aligned perpendicular to the direction of maximum tectonic shortening and parallel to fold axes (e.g. Averbuch *et al.* 1995; Hirt *et al.* 2000; Parés 2015; Fig. 10a). However, AMS k_{max} axes in the Thetford Mines ophiolite plunge steeply to the NE (Fig. 9a) and are demonstrably not related to fold geometries in this way, as fold axes in the ophiolite and associated sedimentary cover sequences are shallowly plunging and oriented NE-SW. Instead, k_{max} axes form a magnetic lineation that is broadly orthogonal to the regional fold axes (Fig. 10b), implying a component of sub-vertical stretching during NW-SE contraction and fabric development.

Deformation processes capable of producing sub-vertical stretching during folding include: (i) flexural flow along fold limbs during shortening; and (ii) transpression (resulting from a combination of pure shear and simple shear deformation). Importantly, Tikoff & Greene (1997) showed that transpression will produce horizontal stretching lineations in systems where the convergence angle is $<20^{\circ}$, but that the long axis of the finite strain ellipsoid (and hence the stretching lineation) will soon become vertical in any high-strain transpressional zone that deviates even slightly from simple shear. Strain modelling indicates that stretching lineations are always vertical for systems with high convergence angles (i.e. undergoing pure shear dominated transpression; Tikoff & Greene 1997).

Both the Taconian and Acadian orogenies in the Canadian Appalachians are known to have been characterized by transpressive regimes. Transpression during Acadian continental collision has

Downloaded from https://academic.oup.com/gji/article-abstract/222/2/1034/5827533 by guest on 02 July 2020

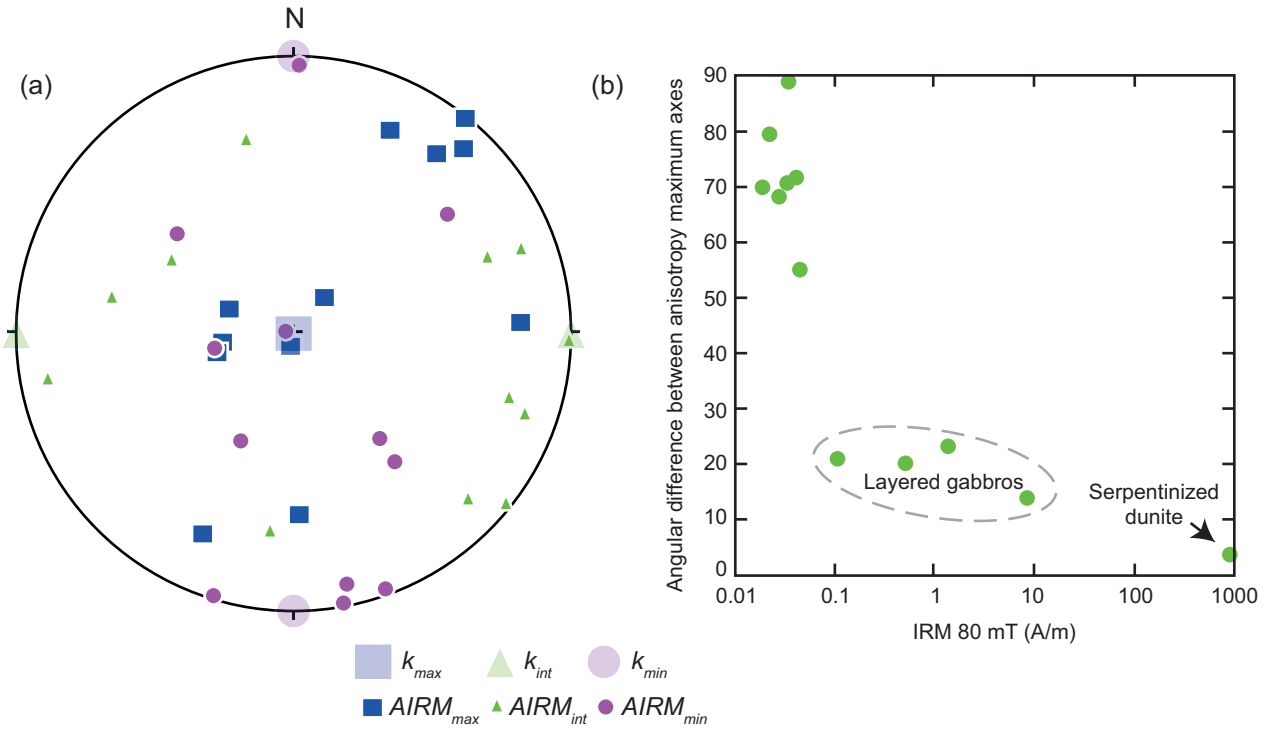

Figure 7. (a) Equal area stereographic projection of AIRM principal axes (small symbols) for selected specimens after rotating the corresponding AMS principal axes to a common reference frame (k_{max} vertical, k_{min} horizontal to the north, k_{int} horizontal to the east; large symbols). Squares/triangle/circles = maximum/intermediate/minimum principal axes of anisotropy, respectively and (b) the relationship between the angular difference between AIRM and AMS maximum principal axes and the intensity of IRM acquired in an 80 mT field.

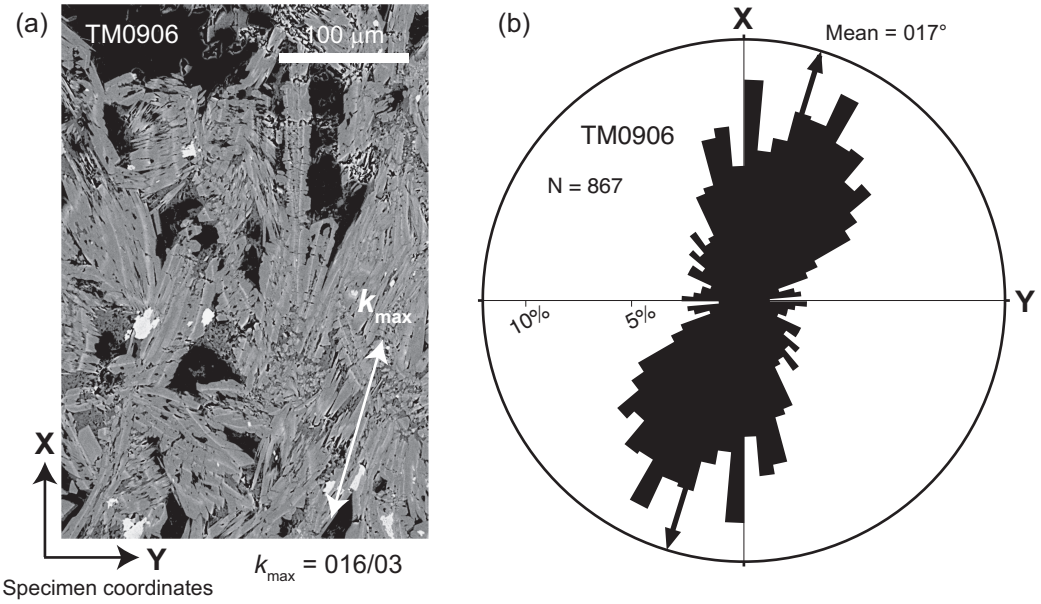

Figure 8. (a) Example of a backscatter SEM image of a pillow lava specimen from the Thetford Mines ophiolite. *K*max for this specimen (white arrow) lies in the X-Y plane; (b) rose diagram showing the preferred orientation of secondary amphibole crystals in the specimen X-Y plane. The mean orientation of 867 measurements of amphibole crystal long-axes (azimuth = 017°; black arrow) is parallel to k_{max} (azimuth = 016°). This is consistent with the AMS signal being carried by paramagnetic amphiboles formed by secondary grain growth during deformation.

been reported in the Gaspé Peninsula (to the NE of the Thetford Mines ophiolite; Malo *et al.* 1995; Sacks *et al.* 2004), in contrast to thrust-dominated, dip-slip tectonics in southern Québec (SW of the ophiolite; Malo *et al.* 1995). These along-strike variations in structural style are interpreted to result from collision during the Devonian of Gondwana-derived terranes with an irregular Laurentian margin inherited from the opening of the Iapetus Ocean (Malo *et al.* 1995; Sacks *et al.* 2004). Further to the SW in the northern

Downloaded from https://academic.oup.com/gji/article-abstract/222/2/1034/5827533 by guest on 02 July 2020

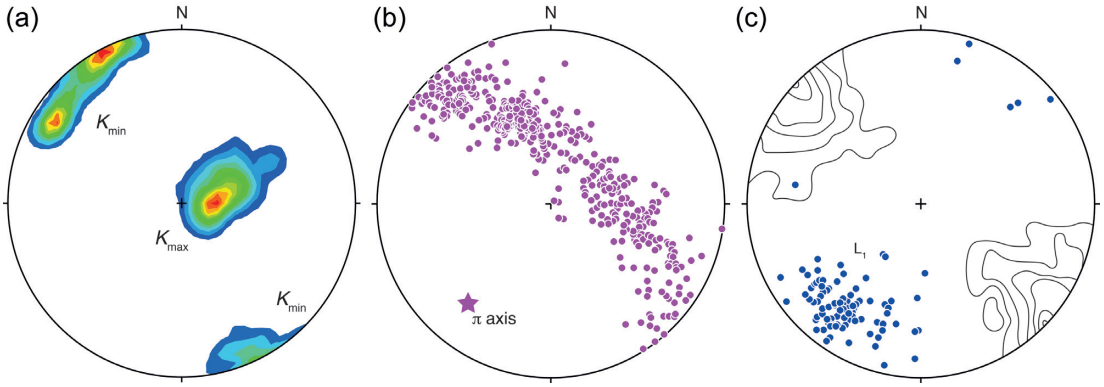

Figure 9. Equal area stereographic projections of: (a) the contoured distributions of k_{min} and k_{max} axes of anisotropy of low-field magnetic susceptibility ellipsoids of samples from the Thetford Mines ophiolite (excluding the layered gabbro locality), showing clusters of NW-SE-oriented shallowly plunging k_{min} axes and NE-oriented steeply plunging k_{max} axes and (b) poles to bedding in the post-emplacement, pre-Acadian sedimentary cover of the ophiolite, defining a girdle distribution indicating a shallowly plunging SW Acadian fold axis orientation. Star = π axis (= 222/23) (data from St-Julien 1987); and (c) L1 fold axes and bedding-cleavage intersection lineations (mean orientation = 217/28) and contoured poles to Acadian cleavage planes (data from St-Julien 1987).

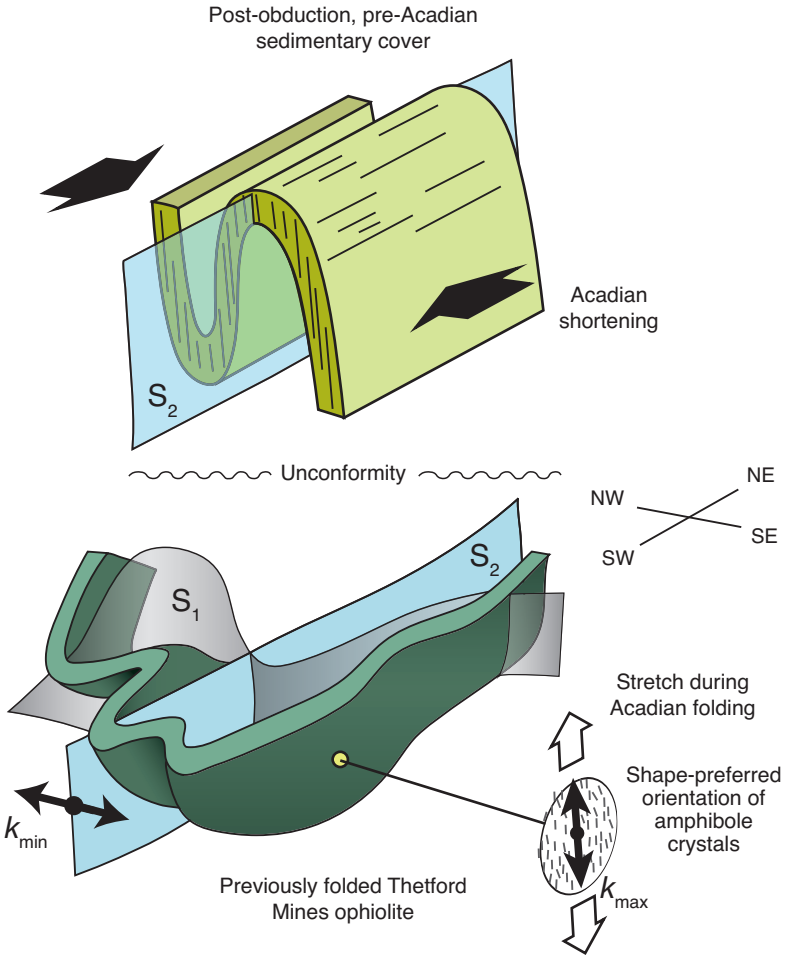

Figure 10. (a) Schematic diagram illustrating the commonly observed relationship between fold geometries and k_{max} axes, whereby k_{max} lies parallel to fold axes and the bedding-cleavage intersection lineation; (b) relationship between fold geometry and k_{max} axes in the Thetford Mines ophiolite, where k_{max} is orthogonal to fold axes, indicating a sub-vertical tectonic stretch inferred to result from deformation in a transpressive setting.

Appalachian region of Maine in the United States, Early Devonian (Acadian) oblique convergence also involved dextral transpression (Solar & Brown 2001). This resulted in dextral, SE-side-up displacement within the Central Maine Belt shear zone system (Solar & Brown 2001). Dextral transpression resulting in vertical stretching lineations has also been reported by Waters-Tormey & Stewart (2010) even further to the SW in the Blue Ridge area of Southern Carolina, with variations in lineation orientation across

Downloaded from https://academic.oup.com/gji/article-abstract/222/2/1034/5827533 by guest on 02 July 2020

this area inferred to result from changes in the effective convergence angle across structural domains (as in Tikoff & Greene 1997).

Given the extensive evidence for Acadian transpression in the Appalachian orogen and the clear correlation between k_{min} orientations and the NW-SE Acadian shortening direction (Fig. 9), we suggest that the sub-vertical stretching implied by the steeply plunging k_{max} axes provides the first evidence for transpressive shear recorded in the Thetford Mines ophiolite. Assuming a pure-shear dominated transpressive regime characterized by NE-SW trending major structures, the orientation of the k_{max} axes would be consistent with dextral shear superimposed on a SE-side-up pure shear component (as observed elsewhere in the Appalachian orogen; Solar & Brown 2001).

5.3 Implications for the interpretation of AMS data in complexly deformed terranes

With the exception of the layered gabbros sampled in the far SW of the study area, AMS results from the Thetford Mines ophiolite provide evidence for complete tectonic obliteration of any magmatic or tectonic fabric that existed prior to the Acadian orogeny. This suggests that the AMS signal in these deformed ophiolitic rocks reflects only the last major stage of the regional strain history. This has also been suggested in a number of other tectonic settings. For example, Anderson & Morris (2004) demonstrated that folded low-grade metasedimentary rocks at Widemouth Bay in the Variscan belt of SW England exhibit AMS fabrics that record late-stage normal faulting, with no record of prior depositional or fold related fabrics. Similarly, Hrouda *et al.* (2014) describe AMS fabrics in an ophiolite in the Bohemian Massif (Czech Republic) that are carried by paramagnetic mafic silicates (including amphiboles and biotite) and that relate to the last exhumation and retrogression event experienced by the ophiolite. Interestingly, Hrouda *et al.* (2014) showed that massive metagabbros in this example suffered only weak deformation and partially preserve intrusive magnetic fabrics, similar to the situation described here.

Finally, we note the potential for erroneous interpretation of the AMS data from any one lithology or site within the Thetford Mines ophiolite, as AMS principal axes at individual sites are observed to coincide with macroscopic magmatic structures (e.g. dyke margins; Fig. 6). Only a comparison of data from multiple sites sampled in different lithologies allows identification of the dominant tectonic overprint in these rocks, highlighting the danger of interpreting results from sites in isolation in complexly deformed terranes.

6 CONCLUSIONS

AMS data are frequently used as a proxy for magmatic and tectonic fabrics in a wide range of rock types in various geological settings (e.g. Borradaile & Jackson 2004; Parés 2015). Previous studies of AMS in ophiolites have been used mainly to examine magmatic fabrics developed during crustal accretion, but the majority of studies have been conducted in Mesozoic ophiolites that have not experienced polyphase deformation during multiple orogenic events. Our data from the Ordovician Thetford Mines ophiolite of the Canadian Appalachians demonstrate that primary magmatic fabrics in more ancient, Palaeozoic ophiolites may be completely obliterated during post-obduction deformation, and may only survive locally in low strain zones. A clear correlation between AMS principal axes and the geometry of Acadian upright folding in the Thetford Mines ophiolite indicates that fabrics in this example record only the last phase of its complex strain history. Importantly, the AMS data provide the first evidence for sub-vertical stretching within the ophiolite related to the transpressional deformation of the Appalachians that has previously only been documented in deformed sedimentary successions.-

ACKNOWLEDGEMENTS

This project was funded by a European Union Horizon 2020 Programme Marie Sklodowska-Curie Actions Individual Fellowship to AdC, Project, 'PASS: Paleozoic Seafloor Spreading'. Stereonets and the rose diagram were produced using 'OSXStereonet' (Cardozo & Allmendinger 2013) and AIRM tensors were analysed using Rick Allmendinger's 'EigenCalc' program.

REFERENCES

Abelson, M., Baer, G. & Agnon, A., 2001. Evidence from gabbro of the Troodos ophiolite for lateral magma transport along a slow-spreading mid-ocean ridge, *Nature,* **409,** 72–75.

Allerton, S. & Vine, F.J., 1991. Spreading evolution of the Troodos ophiolite, Cyprus, *Geology,* **19,** 637–640.

Anderson, M.W. & Morris, A., 2004. The puzzle of axis-normal magnetic lineations in folded low-grade sediments (Bude Formation, SW England), in: *Magnetic Fabric: Methods and Applications,* vol. **238,** pp. 175–190, eds. Martin-Hernandez, F., Lüneburg, C.M., Aubourg, C. & Jackson, M., Geological Society of London Special Publication.

Averbuch, O., Mattei, M., Kissel, C., de Lamotte, D.F. & Speranza, F. 1995. Kinematics of deformations within a blind thrust-system: the example of the ''Montagna dei Fiori'' structure (Central Apennines front, Italy), *Bull. Soc. Geol. Fr.,* **166,** 451–461.

Biedermann, A.R., Bender Koch, C., Pettke, T. & Hirt, A.M., 2015. Magnetic anisotropy in natural amphibole crystals, *Am. Mineral.,* **100,** 1940–1951.

Biedermann, A.R., Kunze, K. & Hirt, A.M., 2018. Interpreting magnetic fabrics in amphibole-bearing rocks, *Tectonophysics,* **722,** 566–576.

Blackman, D.K. *et al.*, 2011. Drilling constraints on lithospheric accretion and evolution at Atlantis Massif, Mid-Atlantic Ridge 30° N, *J. geophys. Res.,* **116,** B07103, doi:10.1029/2010JB007931.

Borradaile, G.J. & Jackson, M., 2004. Anisotropy of magnetic susceptibility (AMS): magnetic petrofabrics of deformed rocks, *Geol. Soc. London Spec. Pub.,* **238,** 299–360.

Borradaile, G.J. & Tarling, D.H., 1981. The influence of deformation mechanisms on magnetic fabrics in weakly deformed rocks, *Tectonophysics,* **77,** 151–168.

Cardozo, N. & Allmendinger, R.W., 2013, Spherical projections with OSXStereonet, *Comput. Geosci.,* **51,** 193–205.

Castonguay, S., Ruffet, G., Tremblay, A. & Féraud, G., 2001. Tectonometamorphic evolution of the southern Québec Appalachians: $^{40}Ar/^{39}Ar$ evidence for Middle Ordovician crustal thickening and Silurian-Early Devonian exhumation of the internal Humber Zone, *Bull. geol. Soc. Am.,* **113,** 144–160.

Hirt, A., Julivert, M. & Soldevila, J., 2000. Magnetic fabric and deformation in the Navia-Alto Sil slate belt, northwestern Spain, *Tectonophysics,* **320,** 1–16.

Housen, B.A., Richter, C. & van der Pluijm, B.A., 1993. Composite magnetic anisotropy fabrics: experiments, numerical models, and implications for the quantification of rock fabrics, *Tectonophysics,* **220**. 1–12.

Hrouda, F., Krejčí, O. & Otava, J., 2000. Magnetic fabric in folds of the easternmost Rheno-Hercynian Zone, *Phys. Chem. Earth (A),* **25,** 505–510.

Hrouda, F, Faryad, S.W, Chlupáčová, M. & Jerábek, P., 2014. Magnetic fabric in amphibolitized eclogites and serpentinized ultramafites in the Mariánské Lázne Complex (Bohemian Massif, Czech Republic): product of exhumation-driven retrogression?, *Tectonophysics,* **629,** 260–274.

Downloaded from https://academic.oup.com/gji/article-abstract/222/2/1034/5827533 by guest on 02 July 2020

Inwood, J., Morris, A., Anderson, M.W. & Robertson, A.H.F., 2009. Neotethyan intraoceanic microplate rotation and variations in spreading axis orientation: paleomagnetic evidence from the Hatay ophiolite (southern Turkey), *Earth planet. Sci. Lett.,* **280,** 105–117.

Jelínek, V., 1978, Statistical processing of magnetic susceptibility measured on groups of specimens, *Stud. Geophys. Geod.,* **22,** 50–62.

Laurent, R. & Hébert, R., 1989. The volcanic and intrusive rocks of the Québec Appalachian ophiolites (Canada) and their island-arc setting, *Chem. Geol.,* **77,** 287–302.

MacLeod, C.J., Allerton, S., Gass, I.G. & Xenophontos, C., 1990. Structure of a fossil ridge-transform intersection in the Troodos ophiolite, *Nature,* **348,** 717–720.

MacLeod, C.J., Dick, H.J.B., Blum, P. & the Expedition 360 Scientists, 2017. *Proceedings of the International Ocean Discovery Program,* Expedition 360: Southwest Indian Ridge Lower Crust and Moho: College Station, TX (International Ocean Discovery Program), doi: 10.14379/iodp.proc.360.2017.

Maffione, M., Morris, A., Plümper, O. & van Hinsbergen, D.J.J., 2014. Magnetic properties of variably serpentinized peridotites and their implication for the evolution of oceanic core complexes, *Geochem. Geophys. Geosyst.,* **15,** 923–944.

Maffione, M., van Hinsbergen, D.J.J., Koornneef, L, Huang, W., Guilmette, C., Ding, L. & Kapp, P., 2015. Forearc hyperextension dismembered the South Tibetan ophiolites, *Geology,* **43,** 475–478.

Malo, M.A., Tremblay, A., Kirkwood, D. & Cousineau, P., 1995. Along-strike Acadian structural variations in the Québec Appalachians: consequence of a collision along an irregular margin, *Tectonics,* **14,** 1327–1338.

Malo, M.A. & Kirkwood, D., 1995. Faulting and progressive strain history of the Gaspé Peninsula in post-Taconian time: a review, in: *Current perspectives in the Appalachian-Caledonian orogen,* vol. **41,** pp. 267–282, eds. Hibbard, J., van Staal, C.R. & Cawood, P.A., Geological Association of Canada Special Paper.

Meyer, M.C., 2015, Magnetic fabric, palaeomagnetic and structural investigation of the accretion of lower oceanic crust using ophiolitic analogues, *PhD thesis (unpublished),* University of Plymouth, 305 pp.

Miller, D.J. & Christensen, N.I., 1997. Seismic velocities of lower crustal and upper mantle rocks from the slow-spreading Mid-Atlantic Ridge, south of the Kane transform zone (MARK), *Proc. Ocean Drill. Prog. Sci. Results,* **153,** 437–454.

Morris, A. & Maffione, M., 2016. Is the Troodos ophiolite (Cyprus) a complete, transform fault-bounded Neotethyan ridge segment?, *Geology,* **44,** 199–202.

Morris, A., Anderson, M.W. & Robertson, A.H.F., 1998. Multiple tectonic rotations and transform tectonism in an intra-oceanic suture zone, SW Cyprus, *Tectonophysics,* **299,** 229–253.

Morris, A., Meyer, M., Anderson, M.W. & MacLeod, C.J., 2016. Clockwise rotation of the entire Oman ophiolite occurred in response to subduction rollback, *Geology,* **44,** 1055–1058.

Olive, V., Hébert, R. & Loubet, M., 1997. Isotopic and trace element constraints on the genesis of boninitic sequence in the Thetford-Mines ophiolitic complex, Quebec, *Can. J. Earth Sci.,* **34,** 1258–1271.

Pagé, P., Bédard, J.H. & Tremblay, A., 2009. Geochemical variations in a depleted fore-arc mantle: the Ordovician Thetford Mines Ophiolite, *Lithos,* **113,** 21–47.

Parés, J.M., 2015. Sixty years of anisotropy of magnetic susceptibility in deformed sedimentary rocks, *Front. Earth Sci.,* **3,** 1–13.

Petrovský, E. & Kapička, A., 2006. On determination of the Curie point from thermomagnetic curves, *J. geophys. Res.,* **111,** B12S27, doi: 10.1029/2006JB004507.

Pinet, N. & Tremblay, A., 1995. Is the Taconian orogeny of southern Quebec the result of an Oman-type obduction?, *Geology,* **23,** 121–124.

Potter, D.K. & Stephenson, A., 1988. Single domain particles in rocks and magnetic fabric analysis, *Geophys. Res. Lett.,* **15,** 1097–1100.

Rochette, P., Jenatton, L., Dupuy, C., Boudier, F. & Reuber, I., 1991. Diabase dikes emplacement in the Oman ophiolite: a magnetic fabric study with reference to geochemistry, in: *Ophiolite Genesis and Evolution of the Oceanic Lithosphere,* pp. 55–82, eds. Peters, T. *et al.*, Ministry of Petroleum and Minerals, Sultanate of Oman.

Sacks, P.E., Malo, M., Trzcienski, W.E., Jr., Pincivy, A. & Gosselin, P., 2004. Taconian and Adadian transpression between the internal Humber Zone and the Gaspé Belt in the Gaspé Peninsula: tectonic history of the Shickshock Sud fault zone, *Can. J. Earth Sci.,* **41,** 635–653.

Schneider, C.A., Rasband, W.S. & Eliceiri, K.W., 2012. NIH Image to ImageJ: 25 years of image analysis, *Nat. Methods,* **9,** 671–675.

Schroetter, J.-M., Tremblay, A., Bédard, J.H. & Villeneuve, M., 2006. Syn-collisional basin development in the Appalachian orogen: the Saint-Daniel mélange, southern Québec, Canada, *Bull. geol. Soc. Am.,* **118,** 109–125.

Solar, G.S. & Brown, M., 2001. Deformation partitioning during transpression in response to Early Devonian oblique convergence, northern Appalachian orogen, USA, *J. Struct. Geol.,* **23,** 1043–1065.

Staudigel, H., Gee, J., Tauxe, L. & Varga, R.J., 1992. Shallow intrusive directions of sheeted dikes in the Troodos ophiolite: anisotropy of magnetic susceptibility and structural data, *Geology,* **20,** 841–844.

St-Julien, P., 1987. Géologie des regions de Saint-Victor et de Thetford Mines (moitié est): Québec, Minstère de l'Energie et des Ressources, MM 86-01, 66 pp.

Tarling, D.H. & Hrouda, F., 1993. *The Magnetic Anisotropy of Rocks,* Chapman & Hall, London, 217 pp.

Thompson, R. & Oldfield, F., 1986. *Environmental Magnetism,* Allen & Unwin, London, 227 pp.

Tikoff, B. & Greene, D., 1997. Stretching lineations in transpressional shear zones: an example from the Sierra Nevada Batholith, California, *J. Struct. Geol.,* **19,** 29–39.

Tremblay, A., Meshi, A. & Bédard, J.H., 2009. Oceanic core complexes and ancient oceanic lithosphere: insights from Iapetan and Tethyan ophiolites (Canada and Albania), *Tectonophysics,* **473,** 36–52.

Tremblay, A. & Castonguay, S., 2002. The structural evolution of the Laurentian margin revisited (southern Quebec): implications for the Salinian Orogeny and Appalachian successor basins, *Geology,* **30,** 79–82.

Tremblay, A. & Pinet, N., 2005. Diachronous supracrustal extension in an intraplate setting and the origin of the Connecticut Valley-Gaspé and Merrimack troughs, Northern Appalachians, *Geol. Mag.,* **142,** 7–22.

Waters-Tormey, C. & Stewart, K., 2010. Heterogeneous wrench-dominated transpression in the deep crust recorded by the Burnsville fault and related structures, Blue Ridge, North Carolina: implications for the Acadian orogeny in the Southern Appalachians, *Geol. Soc. Am. Mem.,* **206,** 917–934.

Whitehead, J., Reynolds, P.H. & Spray, J.G., 1995. The sub-ophiolitic metamorphic rocks of the Québec Appalachians, *J. Geodyn.,* **19,** 325–350.

Whitehead, J., Dunning, G.R. & Spray, J.G., 2000. U–Pb geochronology and origin of granitoid rocks in the Thetford Mines ophiolite, Canadian Appalachians, *Bull. geol. Soc. Am.,* **112,** 915–928.

Williams, H., 1979. Appalachian orogen in Canada, *Can. J. Earth Sci.,* **16,** 792–807.

Yaouancq, G. & MacLeod, C.J., 2000. Petrofabric investigation of gabbros from the Oman ophiolite: comparison between AMS and rock fabric, *Mar. Geophys. Res.,* **21,** 289–305.

SUPPORTING INFORMATION

Supplementary data are available at *GJI* online.

Table S1. Specimen-level AMS results from the Thetford Mines ophiolite.

Table S2. Specimen-level AIRM results from the Thetford Mines ophiolite.

Please note: Oxford University Press is not responsible for the content or functionality of any supporting materials supplied by the authors. Any queries (other than missing material) should be directed to the corresponding author for the paper.

Downloaded from https://academic.oup.com/gji/article-abstract/222/2/1034/5827533 by guest on 02 July 2020

Key words

Authors are requested to choose key words from the list below to describe their work. The key words will be printed underneath the summary and are useful for readers and researchers. Key words should be separated by a semi-colon and listed in the order that they appear in this list. An article should contain no more than six key words.

COMPOSITION and PHYSICAL PROPERTIES
Composition and structure of the continental crust
Composition and structure of the core
Composition and structure of the mantle
Composition and structure of the oceanic crust
Composition of the planets
Creep and deformation
Defects
Elasticity and anelasticity
Electrical properties
Equations of state
Fault zone rheology
Fracture and flow
Friction
High-pressure behaviour
Magnetic properties
Microstructure
Permeability and porosity
Phase transitions
Plasticity, diffusion, and creep

GENERAL SUBJECTS
Core
Gas and hydrate systems
Geomechanics
Geomorphology
Glaciology
Heat flow
Hydrogeophysics
Hydrology
Hydrothermal systems
Infrasound
Instrumental noise
Ionosphere/atmosphere interactions
Ionosphere/magnetosphere interactions
Mantle processes
Ocean drilling
Structure of the Earth
Thermochronology
Tsunamis
Ultra-high pressure metamorphism
Ultra-high temperature metamorphism

GEODESY and GRAVITY
Acoustic-gravity waves
Earth rotation variations
Geodetic instrumentation
Geopotential theory
Global change from geodesy
Gravity anomalies and Earth structure
Loading of the Earth
Lunar and planetary geodesy and gravity
Plate motions
Radar interferometry
Reference systems
Satellite geodesy
Satellite gravity
Sea level change
Seismic cycle
Space geodetic surveys
Tides and planetary waves
Time variable gravity
Transient deformation

GEOGRAPHIC LOCATION
Africa
Antarctica
Arctic region
Asia
Atlantic Ocean
Australia
Europe
Indian Ocean
Japan
New Zealand
North America
Pacific Ocean
South America

GEOMAGNETISM and ELECTROMAGNETISM
Archaeomagnetism
Biogenic magnetic minerals
Controlled source electromagnetics (CSEM)
Dynamo: theories and simulations
Electrical anisotropy
Electrical resistivity tomography (ERT)
Electromagnetic theory
Environmental magnetism
Geomagnetic excursions
Geomagnetic induction
Ground penetrating radar
Magnetic anomalies: modelling and interpretation
Magnetic fabrics and anisotropy
Magnetic field variations through time
Magnetic mineralogy and petrology
Magnetostratigraphy
Magnetotellurics
Marine electromagnetics
Marine magnetics and palaeomagnetics
Non-linear electromagnetics
Palaeointensity
Palaeomagnetic secular variation
Palaeomagnetism
Rapid time variations
Remagnetization
Reversals: process, time scale, magnetostratigraphy
Rock and mineral magnetism
Satellite magnetics

GEOPHYSICAL METHODS
Downhole methods
Fourier analysis
Fractals and multifractals
Image processing
Instability analysis
Interferometry
Inverse theory
Joint inversion
Neural networks, fuzzy logic
Non-linear differential equations
Numerical approximations and analysis
Numerical modelling
Numerical solutions
Persistence, memory, correlations, clustering
Probabilistic forecasting
Probability distributions
Self-organization
Spatial analysis
Statistical methods
Thermobarometry
Time-series analysis
Tomography
Waveform inversion
Wavelet transform

PLANETS
Planetary interiors
Planetary volcanism

SEISMOLOGY
Acoustic properties
Body waves
Coda waves
Computational seismology
Controlled source seismology
Crustal imaging
Earthquake dynamics
Earthquake early warning
Earthquake ground motions
Earthquake hazards
Earthquake interaction, forecasting, and prediction
Earthquake monitoring and test-ban treaty verification
Earthquake source observations
Guided waves
Induced seismicity
Interface waves
Palaeoseismology
Rheology and friction of fault zones
Rotational seismology
Seismic anisotropy
Seismic attenuation
Seismic instruments
Seismic interferometry
Seismicity and tectonics
Seismic noise
Seismic tomography
Site effects
Statistical seismology
Surface waves and free oscillations
Theoretical seismology

Downloaded from https://academic.oup.com/gji/article-abstract/222/2/1034/5827533 by guest on 02 July 2020

Tsunami warning
Volcano seismology
Wave propagation
Wave scattering and diffraction

TECTONOPHYSICS
Backarc basin processes
Continental margins: convergent
Continental margins: divergent
Continental margins: transform
Continental neotectonics
Continental tectonics: compressional
Continental tectonics: extensional
Continental tectonics: strike-slip and transform
Cratons
Crustal structure
Diapirism
Dynamics: convection currents, and mantle plumes
Dynamics: gravity and tectonics
Dynamics: seismotectonics
Dynamics and mechanics of faulting
Dynamics of lithosphere and mantle
Folds and folding
Fractures, faults, and high strain deformation zones
Heat generation and transport
Hotspots
Impact phenomena
Intra-plate processes
Kinematics of crustal and mantle deformation
Large igneous provinces
Lithospheric flexure
Mechanics, theory, and modelling
Microstructures
Mid-ocean ridge processes
Neotectonics
Obduction tectonics
Oceanic hotspots and intraplate volcanism
Oceanic plateaus and microcontinents
Oceanic transform and fracture zone processes
Paleoseismology
Planetary tectonics
Rheology: crust and lithosphere
Rheology: mantle
Rheology and friction of fault zones
Sedimentary basin processes
Subduction zone processes
Submarine landslides
Submarine tectonics and volcanism
Tectonics and climatic interactions
Tectonics and landscape evolution
Transform faults
Volcanic arc processes

VOLCANOLOGY
Atmospheric effects (volcano)
Calderas
Effusive volcanism
Eruption mechanisms and flow emplacement
Experimental volcanism
Explosive volcanism
Lava rheology and morphology
Magma chamber processes
Magma genesis and partial melting
Magma migration and fragmentation
Mud volcanism
Physics and chemistry of magma bodies
Physics of magma and magma bodies
Planetary volcanism
Pluton emplacement
Remote sensing of volcanoes
Subaqueous volcanism
Tephrochronology
Volcanic gases
Volcanic hazards and risks
Volcaniclastic deposits
Volcano/climate interactions
Volcano monitoring
Volcano seismology

Downloaded from https://academic.oup.com/gji/article-abstract/222/2/1034/5827533 by guest on 02 July 2020

© 2017 RAS, *GJI*